ASTROPHYSICAL JOURNAL, IN PRESS
Preprint typeset using LaTeX style emulateapj v. 04/03/99

INTERSTELLAR GAS IN THE NGC 4410 GALAXY GROUP

BEVERLY J. SMITH
CASA, University of Colorado, Box 389, Boulder CO 80309; beverly@casa.colorado.edu[a]

[a]Now at Physics Department, Box 70652, East Tennessee State University, Johnson City TN 37614-0652.

Astrophysical Journal, in press

ABSTRACT

We present new radio continuum, 21 cm HI, and 2.6 mm CO data for the peculiar radio galaxy NGC 4410A and its companion NGC 4410B, and compare with available optical and X-ray maps. Our radio continuum maps show an asymmetric double-lobed structure, with a high surface brightness lobe extending 3.′6 (∼100 kpc) to the southeast and a 6.′2 (∼180 kpc) low surface brightness feature in the northwest. Molecular gas is abundant in NGC 4410A, with $M_{H_2} \sim 4 \times 10^9$ $M_\odot$ (using the standard Galactic conversion factor), but is undetected in NGC 4410B. HI is less abundant, with $M_{HI} \sim 10^9$ $M_\odot$ for the pair. Our HI map shows a 3×10^8 $M_\odot$ HI tail extending 1.′7 (50 kpc) to the southeast of the pair, coincident with a faint optical tail and partially overlapping with the southeastern radio lobe. The HI tail is anti-coincident with a 2′ (56 kpc) long X-ray structure aligned with a stellar bridge that connects the pair to a third galaxy. If this X-ray emission is associated with the group, we infer 3 – 8 $\times 10^8$ $M_\odot$ of hot gas in this feature. This may be either intracluster gas or shocked gas associated with the bridge.

Our detection of abundant interstellar gas in this pair, including an HI-rich tidal tail near the southeastern radio lobe, suggests that the observed distortions in this lobe may have been caused by the interstellar medium in this system. The gravitational interaction of the two galaxies and the subsequent motion of the interstellar medium in the system relative to the jet may have produced sufficient ram pressure to bend and distort the radio jet. An alternative hypothesis is that the jet was distorted by ram pressure due to an intracluster medium, although the small radial velocity of NGC 4410A relative to the group and the lack of diffuse X-ray emission in the group makes this less likely unless the group is not virialized or is in the process of merging with another group.

Using our VLA data, we also searched for HI counterparts to the other ten known members of the NGC 4410 group and CO from three other galaxies in the inner group. In our velocity range of 6690 km s^{-1} – 7850 km s^{-1}, we detected six other galaxies above our HI sensitivity limits of 2×10^8 $M_\odot$ for the inner group and 4×10^8 $M_\odot$ for the outer group. The total HI in the group is 1.4×10^{10} $M_\odot$, 80% of which arises from four galaxies in the outer group. Three of these galaxies (VCC 822, VCC 831, and VCC 847) are spirals with M_{HI}/L_B ratios typical of field galaxies, while FGC 170A appears to be a gas-rich dwarf galaxy ($M_B \sim -18$; $M_{HI} \sim 3 \times 10^9$ $M_\odot$). In the inner group, the SBa galaxy NGC 4410D (VCC 934) was detected in HI and CO ($M_{HI} \sim 5 \times 10^8$ $M_\odot$ and $M_{H_2} \sim 8 \times 10^8$ $M_\odot$) and has a 1′ (28 kpc) long HI tail that points towards the nearby disk galaxy NGC 4410F. NGC 4410F was also detected in HI ($M_{HI} \sim 4 \times 10^8$ $M_\odot$). The galaxies in the inner group appear to be somewhat deficient in HI compared to their blue luminosities, suggesting phase changes driven by galaxy-galaxy or galaxy-intracluster medium encounters.

Subject headings: Galaxies: Individual (NGC 4410) – Galaxies: ISM – Galaxies: Interactions

1. INTRODUCTION

1.1. *The Interstellar Medium in Radio Galaxies*

There is increasing evidence that the large radio structures found near luminous radio galaxies both affect and are affected by their environment. They may be distorted by motion through an intracluster medium (Miley et al. 1972; O'Dea & Owen 1985), or by an encounter with the interstellar medium in the host galaxy (e.g., de Young 1981; van Breugel et al. 1984, 1985a), a companion galaxy (Stocke, Burns, & Christiansen 1985; Borne & Colina 1993; Harris, Leighly, & Leahy 1998), or a galaxy in the process of merging with the host galaxy (van Breugel et al. 1986). A gravitational encounter between two galaxies or clusters of galaxies may disrupt previously-existing radio lobes by perturbing the interstellar or intracluster medium (Comins & Owen 1991; Borne & Colina 1993). In some systems, an impact between a jet and the interstellar medium appears to have triggered star formation (de Young 1981; van Breugel et al. 1985b; van Bruegel & Dey 1993; Graham 1998).

To investigate the interplay between the radio lobes and the interstellar medium in radio galaxies, detailed studies of the interstellar matter in nearby radio galaxies are essential. Although there have been a number of narrowband optical imaging surveys of radio galaxies (e.g., Hansen, Norggard-Nielsen, & Jorgensen 1987; Baum et al. 1988; Morganti, Ulrich, & Tadhunter 1992; McCarthy et al. 1995; Hes, Barthel, & Fosbury 1996), measuring the distribution of ionized gas in more than 100 radio galaxies, studies of the neutral gas in radio galaxies have been scarce. A few pioneering single-dish searches for the 21 cm HI line (Dressel, Bania, & O'Connell 1982; Bieging & Biermann 1983; Jenkins 1983) and the 2.6 mm CO line (Mirabel et al. 1989; Mazzarella et al. 1993) in radio galaxies have detected only a handful of radio galaxies. There have been a number of high resolution interferometric studies of HI absorption towards the nuclei of radio galaxies (e.g., van Gorkom et al. 1989), however, the large-scale distribution of

HI emission has been successfully mapped in only a handful of radio galaxies, including Centaurus A (van Gorkom et al. 1990; Schiminovich et al. 1994), NGC 1052 (van Gorkom et al. 1986), NGC 4278 (Raimon et al. 1981; Lees 1992), and PKS B1718-649 (Véron-Cetty et al. 1995).

In this paper, we present a detailed study of the interstellar matter in the nearby low luminosity radio galaxy NGC 4410A and its companions, and compare with other radio galaxies. Throughout this paper we use a Hubble constant of H_o = 75 km s^{-1} Mpc^{-1}.

1.2. *NGC 4410*

Optical images of NGC 4410A, classified as an Sab ? Pec galaxy by de Vaucouleurs et al. (1991), reveal a prominent bulge surrounded by an extended ring or loop-like structure (Hummel et al. 1986). This structure is clearly visible in Figure 1a, a broadband red Hubble Space Telescope (HST) archival image[1] of NGC 4410A. In this image, a number of bright knots are apparent in the eastern half of the ring, and an especially luminous knot is visible southeast of the nucleus. Narrowband Hα+[N II] imaging and optical spectroscopy show that these knots are extremely luminous H II region complexes with $L_{H\alpha}$ $\sim 10^{40} - 10^{41}$ erg s^{-1} (Donahue et al. 2000). The western portion of this ring contains filamentary ionized gas which appears to be shock-ionized (Donahue et al. 2000). The presence of interstellar dust is apparent in the HST image; beautiful filamentary dust lanes are visible southeast of the nucleus and along the eastern half of the ring, extending into the center of the galaxy.

NGC 4410A is strongly interacting with the nearby galaxy NGC 4410B (Figure 1b; Donahue et al. 2000), which has been classified as S0 ? Pec (de Vaucouleurs et al. 1991) or E (Hummel, Kotanyi, & van Gorkom 1986). These two galaxies are part of a sparse group containing at least a dozen galaxies which lies behind the Virgo cluster (Table 1a). The inner 10′ diameter of this group contains five of these galaxies, at least four of which are strongly interacting (Figure 1c; Donahue et al. 2000). NGC 4410A+B may be connected by a stellar bridge to the S0 galaxy NGC 4410C (IC 790), which in turn is connected to the SBa galaxy NGC 4410D (VCC 934). In addition to the possible bridge to NGC 4410C, NGC 4410A+B has a long (2′ $\sim$ 55 kpc) tail to the southeast and another extension to the northwest (Hummel et al. 1986; Figure 1c). A larger field of view (30′ diameter) optical picture of the NGC 4410 group is presented in Figure 1d, where the Digitized Sky Survey[2] (DSS) optical image is shown. Table 1a contains the twelve known galaxies in the inner 30′ diameter of the NGC 4410 group, Table 1b gives foreground and background galaxies in the NGC 4410 field, and Table 1c lists additional galaxies in the field with unknown redshifts. These 27 galaxies are identified in Figure 1d.

Both NGC 4410A and NGC 4410B have been classified as 'Low Ionization Nuclear Emission Region' (LINER) galaxies based on their optical spectra (Mazzarella & Boroson 1993; Donahue et al. 2000). NGC 4410A+B has a 4.8 GHz luminosity of 1.5×10^{23} W Hz^{-1} (Condon, Frayer, & Broderick 1991). This luminosity is near the dividing line between starbursts and radio-loud active galaxies. Galaxies in which the radio continuum is powered by star formation, as indicated by a high infrared to radio continuum ratio, have $L_{4.8\ GHz} \leq 10^{23}$ W Hz^{-1} and tend to be spirals, while systems with higher radio luminosities have lower FIR/radio ratios, indicating radio-loud active nuclei, and tend to be classified as elliptical or S0 (Condon et al. 1991). The NGC 4410A+B pair has a far-infrared luminosity (as in Lonsdale et al. 1985) of 3.9×10^9 $L_\odot$ (Mazzarella, Bothun, & Boroson 1991), giving a far-infrared to 4.8 GHz luminosity ratio (as in Condon et al. 1991) of $\sim$2.8, two orders of magnitude less than that expected for starbursts (Condon et al. 1991), placing it firmly in the radio galaxy class.

Radio continuum maps of NGC 4410A+B show that most of the radio emission originates from a very large (4.′5 $\times$ 3′; 120 kpc $\times$ 80 kpc) knotty structure extending to the southeast of NGC 4410A+B (Hummel et al. 1986; Batuski et al. 1992). A compact radio continuum source coincident with the optical nucleus of NGC 4410A is also observed, indicating that NGC 4410A is the source of the radio emission. This peculiar radio structure has been attributed to the motion of a low luminosity radio galaxy through intracluster gas (Stocke & Burns 1987), or to a low luminosity radio galaxy disturbed by an interaction (Hummel et al. 1986).

The NGC 4410 group was observed at energies between 0.1 and 2.4 keV by the ROSAT X-ray satellite, using both the High Resolution Imager (HRI) and Position Sensitive Proportional Counter (PSPC) (Tschöke, Hensler, & Junkes 1999). The HRI map shows a point-like source associated with NGC 4410A and a diffuse halo extending 10″ to the southeast, while the low resolution PSPC map shows some faint diffuse emission extending eastward from the NGC 4410A+B pair. The PSPC X-ray spectrum of NGC 4410A+B can be deconvolved into two components, a power-law spectrum and a Raymond-Smith spectrum, presumably arising from the compact and extended sources, respectively.

To better understand the relationship between the interaction, the radio emission, and the interstellar medium in the NGC 4410 group, we have obtained new radio continuum, 21 cm HI, and CO (1 – 0) observations of this group, and have compared these with available optical and X-ray data. In Section 2 of this paper, we describe the observations and data reduction. In Section 3, we summarize the results, which are discussed in detail in Section 4. Conclusions are given in Section 5.

2. OBSERVATIONS AND DATA REDUCTION

2.1. *The 21 cm HI Observations*

The NGC 4410 group was observed in the 21 cm HI line using the D configuration of the NRAO[3] Very Large Array on 1997 December 22. The two IF mode was used with 31 195 kHz channels and on-line Hanning smoothing, giving a spectral resolution of 43 km s^{-1} and a total bandpass of 1330 km s^{-1}, centered on a velocity of 7252 km s^{-1}. The total on-galaxy observing time was 8 hours. During this observing run, 3C 286 was observed for 20 minutes for flux and bandpass calibration, and a nearby phase calibrator was observed every 30 minutes for 5 minutes.

The data were calibrated and maps were made using the

[1]Based on observations made with the NASA/ESA Hubble Space Telescope, obtained from the data archive at the Space Telescope Science Institute. STScI is operated by the Association of Universities for Research in Astronomy, Inc. under NASA contract NAS 5-26555.

[2]The Digitized Sky Survey was produced at the Space Telescope Science Institute under U.S. Government grant NAG W-2166. This image is a digitized version of a photographic plate from the Second Palomar Observatory Sky Survey (POSS-II) made by the California Institute of Technology with funds from the National Science Foundation, the National Geographic Society, the Sloan Foundation, the Samuel Oshin Foundation, and the Eastman Kodak Corporation.

[3]The National Radio Astronomy Observatory is a facility of the National Science Foundation, operated under cooperative agreement by Associated Universities, Inc.

NRAO Astronomical Image Processing System (AIPS). After calibration, the AIPS task UVLIN was utilized to remove the continuum, and CLEANed line-only datacubes were produced using the AIPS routine IMAGR. Inspection of these channel maps shows that eight galaxies in the field were detected in HI (see Table 2) and line emission is present in 22 channels, from 6777 – 7685 km s^{-1} (see Sections 3.2 and 3.3). To best isolate the HI emission from the different galaxies in the field, the continuum subtraction process was done four times, using four different sets of continuum channels. These four sets of maps were then combined into a single cube, selecting the appropriate region around each galaxy. For highest sensitivity, a set of maps was made with natural weighting, giving a beamsize of $59\farcs38 \times 54\farcs67$ and an rms of 0.21 mJy beam^{-1} channel^{-1}. Higher resolution maps were also made using the Briggs (1995) robustness weighting scheme with different robustness parameters. These additional maps did not show significantly different morphologies, and so are not discussed further here.

A final continuum map was made by combining the line-free channels at the ends of the bandpass. The final CLEANed, primary beam-corrected, naturally-weighted continuum map of the NGC 4410 field is superposed on the optical DSS image in Figure 2. The noise level in this map is 0.17 mJy beam^{-1} (4.6×10^{-5} mJy arcsec^{-2}), compared to 0.13 mJy beam^{-1} (3.1×10^{-4} mJy arcsec^{-2}) in the higher resolution Hummel et al. (1986) C Array map. The inner portion of the channel maps, showing the central five galaxies of the NGC 4410 group, is presented in Figure 3.

We created moment maps using the AIPS routine MOMNT. For these maps, a scratch copy of the data cube was convolved with a $60''$ Gaussian. Only pixels above 0.4 mJy beam^{-1} in this smoothed cube were including in deriving an HI intensity map from the original unsmoothed data cube. To construct an HI velocity map, a flux cutoff of 0.7 mJy beam^{-1} was used. These moment maps were then corrected for primary beam attenuation.

The naturally-weighted HI intensity map of the inner portion of the NGC 4410 field is displayed in Figure 4a, superposed on the Donahue et al. (2000) R band image. For comparison, the radio continuum map and the low resolution ROSAT PSPC X-ray map from Tschöke et al. (1999) are also overlaid on the optical map in Figure 4b, along with the HI map. In Figure 5, a larger field of view HI intensity map is overlaid on the optical DSS image, and the global HI spectra for the detected galaxies are plotted in Figure 6.

In Table 2, we provide the HI line fluxes for the detected galaxies in the group, their central velocities, and their line widths, along with upper limits for the other group galaxies in the observed velocity range. The HI masses for the detected galaxies range from 4×10^8 M$_\odot$ – 10^9 M$_\odot$ for the galaxies in the inner core of the group, to $2 – 3 \times 10^9$ M$_\odot$ for the four outer galaxies. These masses are provided in Table 4, along with the blue luminosities and M$_{HI}$/L$_B$ ratios.

2.2. *The CO (1 – 0) Observations*

Six positions in the NGC 4410 system were observed in the 2.6mm CO (1 – 0) line during 1997 April and May, 1998 June, and 1999 January, February, and November, using the 3mm SIS receiver on the NRAO 12m telescope. These six positions are the centers of the five innermost galaxies in the group (NGC 4410A, B, C, D, and F) and a position in the southeastern HI tail of NGC 4410A+B (Table 3). Two 256×2 MHz filterbanks, one for each polarization, were used for these observations, providing a total bandpass of 1330 km s^{-1} with a spectral resolution of 5.2 km s^{-1}. The positions and central velocities used for these observations are those tabulated in Table 1. A nutating subreflector with a beam throw of $3'$ in the azimuthal direction ($1'$ for NGC 4410F) was used for these observations, taking care to avoid chopping on other galaxies, tails, or bridges in the group. Each scan was 6 minutes long. The beamsize FWHM is $55''$ at 115 GHz. The pointing was checked hourly using 3C 273 and was consistent to $10''$. The system temperatures ranged from 300 to 400 K. Calibration was accomplished using an ambient temperature chopper wheel.

The CO spectra for all six observed positions are displayed in Figure 7. CO was detected in NGC 4410A and NGC 4410D, but was not found towards NGC 4410B, NGC 4410C, NGC 4410F, or the NGC 4410A+B tail. The CO line fluxes are given in Table 3, along with the central velocities of the lines, the line widths, and the rms noise levels. In Table 4, the molecular gas masses and upper limits for the observed galaxies in the group are given, calculated assuming the standard Galactic I$_{CO}$/N$_{H_2}$ ratio (Bloemen et al. 1986).

3. RESULTS

3.1. *NGC 4410A+B*

3.1.1. *The Radio Continuum Map*

As noted earlier, the radio continuum morphology of NGC 4410A+B is highly peculiar. The VLA C Array observations of Hummel et al. (1986) showed a knotty distorted structure extending $4\farcm5$ (120 kpc) to the southeast of the optical galaxies. This feature is also visible in our new D Array data (Figure 2 and Figure 4b). In addition, our data has revealed the existence of another much lower surface brightness feature, extending $6\farcm2$ (180 kpc) to the northwest of NGC 4410A (Figure 2). Like the southern lobe, the northern feature is distorted. The ridge that connects this lobe to the southern lobe is offset to the east with respect to NGC 4410A.

Our data gives a total 20 cm continuum flux from NGC 4410A+B of 403 ± 11 mJy, with 23 ± 7 mJy of this coming from the northern lobe. For comparison, Kotanyi (1980) and Hummel et al. (1986) found 20 cm flux densities for NGC 4410A+B of 392 ± 21 mJy (as corrected by Hummel et al. 1986) and 340 ± 30 mJy, respectively.

3.1.2. *The 21 cm HI Data*

The distribution of interstellar gas in NGC 4410A+B is strongly disturbed (Figure 4a). The peak of the HI distribution lies $\sim 25''$ to the southeast of NGC 4410A, in the direction of the prominent H II region visible in the Hubble Space Telescope image (Figure 1a). Extending to the southeast of this peak is a tail $1\farcm7$ (50 kpc) long, containing M$_{HI} \sim 3 \times 10^8$ M$_\odot$. This gaseous structure is associated with a faint optical tail (Figure 4a). A second structure containing M$_{HI} \sim 10^8$ M$_\odot$ extends $\sim 0\farcm5$ (14 kpc) to the east of the optical galaxies, near the stellar bridge connecting the pair with NGC 4410C. A third extension containing M$_{HI} \sim 10^8$ M$_\odot$ lies $\sim 1'$ (28 kpc) due south of the pair. The total HI line flux for NGC 4410A+B is 0.55 ± 0.15 Jy km s^{-1}, corresponding to 1.3×10^9 M$_\odot$ of atomic hydrogen. This measurement is consistent with previously-published single-dish fluxes of $\leq$0.51 Jy km s^{-1} (Bieging & Biermann 1983) and 0.74 Jy km s^{-1} (Hoffman et al. 1989), both made with the Arecibo $3\farcm2$ beam.

Although both the radio continuum and HI line emission of NGC 4410A+B extend to the southeast of NGC 4410A+B,

their detailed distributions are different (Figure 4b). The HI is distributed in a narrow tail-like structure extending southwest, with two shorter extensions to the south and east. The continuum is more widely distributed than the HI gas, extending further in the east-west direction, although it has a similar north-south size.

The HI spectrum for NGC 4410A+B (Figure 6) shows a peak at ∼7350 km s^{-1}, close to the optical velocity of NGC 4410A (7440 km s^{-1}; Table 1). NGC 4410A+B also has a second weaker HI peak at ∼7140 km s^{-1}, near the optical velocity of the luminous HII region to the southeast of NGC 4410A and the H II regions in the ring (Donahue et al. 2000). The VLA line width and the observed velocity range for NGC 4410A+B are consistent with those of the single-dish spectrum of Hoffman et al. (1989).

The HI velocity field of NGC 4410A+B is very disturbed. Because of these peculiarities, the velocity structure is better seen in the channel maps (Figure 3) than in standard intensity-weighted first moment maps. In Figure 3, the NGC 4410A+B HI tails are visible as $3-5\sigma$ structures between 7295 km s^{-1} and 7382 km s^{-1}. The southeastern tail is somewhat blueshifted (7295 – 7338 km s^{-1}) with respect to the feature extending due south (7382 km s^{-1}). Another 5σ clump at the end of southeastern tail is blueshifted 130 km s^{-1} from the rest of the tail to 7166 km s^{-1}. The central HI component is visible from 7122 – 7382 km s^{-1}, from the optical velocity of the NGC 4410A nucleus (7440 km s^{-1}) to the velocities of the H II regions southeast of the nucleus and in the ring (7140 – 7300 km s^{-1}; Donahue et al. 2000).

3.1.3. *The Molecular Gas*

The CO line was detected towards NGC 4410A but not towards NGC 4410B or the observed position in the southeastern HI tail (Figure 7). Thus the molecular gas in this pair is concentrated in NGC 4410A. The CO line of NGC 4410A is very broad, covering a total velocity range of ∼750 km s^{-1}, from 7000 km s^{-1} to 7750 km s^{-1}. This spectum has three peaks, at ∼7140, 7300, and 7565 km s^{-1}. The first two velocity components have HI counterparts (Figure 6a); the high velocity feature at 7565 km s^{-1} does not. The ionized gas, however, covers a velocity range similar to that of the CO (Donahue et al. 2000). In the eastern portion of the NGC 4410 ring, the H II regions have optical velocities between 7140 km s^{-1} and 7300 km s^{-1}, while the shock-ionized gas in the western part of the ring has an optical velocity of 7500 km s^{-1} (Donahue et al. 2000). The optical ring lies entirely in the CO beam, therefore, it is possible that the low velocity CO gas lies in the eastern portion of the ring and is associated with the star formation regions, while the high velocity molecular gas is associated with the western filamentary feature. However, the nucleus of NGC 4410A has broad optical lines (FWHM ∼ 600 km s^{-1}; Donahue et al. 2000), so we cannot rule out a more concentrated location for the molecular gas. NGC 4410A+B has a total H_2 mass of 3.9×10^9 $M_\odot$; about 40% of this is in the high velocity component at 7565 km s^{-1}.

3.1.4. *The X-Ray Distribution*

The difference between the HI and X-ray morphologies of NGC 4410A+B is remarkable (Figure 4b). In the X-ray map, a faint elongation extending 2′ (56 kpc) to the east of the NGC 4410A nucleus is apparent. This lies along the stellar bridge connecting NGC 4410A+B with NGC 4410C. In contrast, the extended HI is found mainly along the southeastern tail of NGC 4410A+B rather than the bridge, although there is a hint of a HI extension near the base of the X-ray extension, near the optical bridge.

The X-ray feature is detected at a $3–8\sigma$ level above the X-ray background, at $4 - 10 \times 10^{-7}$ counts s^{-1} arcsec^{-2}. Assuming a 1 keV Raymond-Smith plasma and the Galactic N_H value of 1.7×10^{20} cm^{-2} (Dickey & Lockman 1990), we find an unabsorbed 0.1 – 2.4 keV surface brightness in the bridge of $5 - 13 \times 10^{-18}$ erg s^{-1} cm^{-2} arcsec^{-2}, using the on-line PIMMS conversion tool (Mukai 1993). If this extended emission is indeed associated with the group (see Section 4.1), it has an X-ray luminosity of 4×10^{40} erg s^{-1}, ∼10% of the total X-ray luminosity of NGC 4410A+B.

3.2. *NGC 4410D*

The barred galaxy NGC 4410D was also detected in HI and CO, with $M_{HI} \sim 5 \times 10^8$ $M_\odot$ and $M_{H_2} \sim 8 \times 10^8$ $M_\odot$. Like NGC 4410A+B, NGC 4410D has a peculiar HI morphology and velocity structure. There is a long HI tail extending 1′ (28 kpc) south from NGC 4410D towards NGC 4410F, aligned with a faint stellar feature (Figure 4a). This structure contains M_{HI} $\sim 2 \times 10^8$ $M_\odot$. There is also a second concentration of HI associated with the main disk of this galaxy, with a slight (∼0.′5 ∼ 14 kpc) extension northwards from the eastern edge of NGC 4410D.

The HI spectrum of NGC 4410D shows two distinct features, both with relatively narrow (FWHM ∼ 90 km s^{-1}) line widths: one near the optical velocity at 6960 km s^{-1} and a second at 7380 km s^{-1} (Figure 6a). These two velocity components are spatially separated: the component at 7382 – 7425 km s^{-1} is associated with the southern tail, while the gas at 6907 – 6993 km s^{-1} is associated with the optical disk and northern extension. The CO line of NGC 4410D (Figure 7) has a peak velocity of 6960 km s^{-1}, consistent with the low velocity HI peak and the optical value.

3.3. *NGC 4410F*

The small galaxy NGC 4410F was detected in HI but not in CO, with $M_{HI} \sim 4 \times 10^8$ $M_\odot$ and $M_{H_2} \leq 5 \times 10^8$ $M_\odot$. The HI distribution of NGC 4410F appears somewhat disturbed, being slightly elongated to the south (Figure 4a). NGC 4410F has such a narrow HI line (Figure 6a) that it is almost unresolved at our velocity resolution; it is detected above 3σ in only two channels (Figure 3).

3.4. *The Outer Galaxies in the NGC 4410 Group*

In addition to NGC 4410A+B, NGC 4410D, and NGC 4410F, four galaxies in the outskirts of the NGC 4410 group were detected in HI: VCC 822, VCC 831, VCC 847, and FGC 170A (Figure 5). These galaxies have more regular HI distributions and velocity fields than the galaxies in the inner group. The intensity-weighted HI velocity maps for these galaxies are shown in Figures 8a-d, superposed on the optical DSS images. These maps show evidence of rotation and lines of nodes consistent with the optical position angles.

These four galaxies have higher M_{HI}/L_B ratios than the galaxies in the inner group (Table 4). VCC 822, VCC 831, and VCC 847 have $M_{HI}/L_B \sim 0.12 - 0.26$ $M_\odot/L_\odot$, typical of field spirals (Haynes & Giovanelli 1984). FGC 170A has the highest M_{HI}/L_B ratio of the group, 1.2 $M_\odot/L_\odot$, and the lowest blue luminosity, 2×10^9 $L_\odot$. This corresponds to an absolute B magnitude of ∼–18, similar to that of the Large Magellanic Cloud.

4. DISCUSSION

4.1. *Comparison with Other Radio Galaxies*

Our detection of a second large radio continuum structure near NGC 4410 confirms that this galaxy is indeed a double-lobed radio galaxy, albeit with a distorted radio morphology. The peculiar ring-like optical structure of NGC 4410A, along with the existence of the optical and/or HI tails/bridges extending from the NGC 4410A+B pair, indicates that these galaxies have been gravitationally disturbed by a collision or close encounter. The hosts of radio galaxies are generally elliptical or elliptical-like (e.g., Lilly & Prestage 1987; Owen & White 1991). A number of recent studies have claimed a higher rate of morphological peculiarities in radio galaxy hosts compared to radio-quiet ellipticals (Heckman et al. 1986; Colina & de Juan 1995; Zirbel 1996), although this conclusion is controversial (Ledlow & Owen 1995). The peculiar optical morphology of NGC 4410A is therefore unusual for a radio galaxy but perhaps not unique.

The HI morphologies and velocity structures of the galaxies in the inner core of the NGC 4410 group are quite peculiar compared with normal disk galaxies. At least two HI tails are detected, both with optical counterparts. The presence of these stellar counterparts indicates that the HI distortions are not due to ram pressure stripping by intracluster gas; tidal interactions between the galaxies are probably predominantly responsible for these structures. The five galaxies in the inner core are quite deficient in HI relative to their blue luminosities, compared with field spirals (e.g., Haynes & Giovanelli 1984). The tail-like features in this group are not particularly rich in HI ($M_{HI} \sim 1-4 \times 10^8$ $M_\odot$) compared with other tidal tails, which sometimes have $M_{HI} \sim 10^9$ $M_\odot$ (e.g., Smith 1991; Hibbard & van Gorkom 1996; Duc et al. 1997). The southeastern tail of NGC 4410A+B has a blue magnitude of $\sim 2 \times 10^9$ $L_\odot$ (Donahue et al. 2000), giving $M_{HI}/L_B \sim 0.2$ $M_\odot/L_\odot$ for this feature, similar to the tails studied by Smith (1991) and Hibbard & van Gorkom (1996).

The molecular gas mass of NGC 4410A (4×10^9 $M_\odot$) and its broad (FWHM ~ 600 km s^{-1}) CO line are not unusual for a radio galaxy. Out of the ten radio galaxies surveyed by Mirabel et al. (1989) and Mazzarella et al. (1993), seven have CO luminosities similar to that of NGC 4410A, some with similarly broad lines. In contrast to the radio galaxies in these two surveys, however, NGC 4410A+B has a low L_{FIR}/M_{H_2} ratio of ~ 1 $L_\odot/M_\odot$, indicating a lower rate of star formation compared with the available molecular gas.

It is not clear at present whether the amount of HI in NGC 4410A+B, 10^9 $M_\odot$, is high compared with other radio galaxies, or if the presence of the HI tail is unusual in a radio galaxy. The few single-dish HI emission-line surveys of radio galaxies done to date (Dressel et al. 1982; Bieging & Biermann 1983; Jenkins 1983) have not been sensitive enough to provide strong constraints on the HI masses of radio galaxies. Although a number of high spatial resolution HI absorption studies of radio galaxies have been done (e.g., van Gorkom et al. 1989), only a handful of HI emission line maps of radio galaxies have been published to date. Centaurus A has a warped HI disk (van Gorkom et al. 1990) and HI associated with 'shells' (Schiminovich et al. 1994), NGC 4278 has a large rotating disk of HI (Raimond et al. 1981; Lees 1992), NGC 1052 and PKS B1718-649 have extended HI disks with tidal features (van Gorkom et al. 1986; Véron-Cetty et al. 1995), while Pictor A, PKS 0349-27, and PKS 0634-20 were undetected in HI with the VLA (Simkin & Callcut 1996).

The X-ray morphology of NGC 4410A+B is rather unusual. The only other galaxy with a possible X-ray counterpart to a tidal feature is the radio galaxy Fornax A (Mackie & Fabbiano 1998). The tails of the eight non-radio galaxy mergers studied by Hibbard et al. (1994), Read, Ponman, & Wolstencroft (1995) and Read & Ponman (1998) were not detected by ROSAT. In both the Fornax A feature and the NGC 4410 bridge, the X-rays appear to be due to hot gas rather than X-ray binaries associated with the stellar population in the tidal feature. The blue luminosity of the bridge between NGC 4410A+B and NGC 4410C is 2×10^9 $L_\odot$ (Donahue et al. 2000), giving $L_X/L_B \sim 2 \times 10^{31}$ erg s^{-1}/$L_\odot$. This ratio is $\sim$75 times higher than that found for normal spiral galaxies (Fabbiano, Kim, & Trinchieri 1992) indicating that this X-ray emission is not due to X-ray binaries.

The possibility that the X-ray 'tail' near NGC 4410 is due to hot gas outflowing from the luminous star formation regions and/or the active nucleus, coincidently superposed on an unrelated stellar bridge, also appears to be ruled out by the large X-ray luminosity and size of this feature. A single-sided X-ray outflow with similar luminosity and size has been found near the 'ultraluminous' galaxy Arp 220 (Heckman et al. 1996) and interpreted as the result of a 'superwind' from a starburst or quasar. However, Arp 220 has a far-infrared luminosity 100 times higher than NGC 4410A+B (Smith & Harvey 1996), indicating a much higher star formation rate and/or stronger nuclear activity than in NGC 4410A. Better galaxies to compare with NGC 4410A are the edge-on starbursts M82 and NGC 253, which have far-infrared luminosities about five times that of NGC 4410A+B (Rice et al. 1988). The outflows from these two galaxies have X-ray extents of only $\sim 10-15$ kpc and X-ray luminosities an order of magnitude lower than that of the NGC 4410 'tail' (Fabbiano 1988; Bregman, Schulman, & Tomisaka 1995; Read, Ponman, & Strickland 1997; Dahlem, Weaver, & Heckman 1998). This argues that the extended X-ray structure near NGC 4410A+B is not due to a galactic wind.

It is possible that the extended X-ray emission near NGC 4410 is due to background or foreground sources or coincidently superposed intracluster gas unrelated to the bridge. ROSAT maps of other groups and poor clusters often show asymmetric distorted X-ray morphologies (Doe et al. 1995; Pildis, Bregman, & Evrard 1995; Mulchaey et al. 1996; Mulchaey & Zabludoff 1998). An alternative hypothesis is that the X-rays are arising from tidal gas shocked and heated during the interaction between the two galaxies, as suggested for the X-ray emitting gas in the Fornax A features by Mackie & Fabbiano (1998). The spatial coincidence of the X-ray feature and the optical bridge in NGC 4410 is excellent (Figure 4b), suggesting an association. Using standard X-ray cooling functions (McKee & Cowie 1977; McCray 1987) and assuming a face-on flattened cylinder with an axial ratio between 0.1 and 1, the mass of X-ray emitting gas in the NGC 4410 extension is $3-8 \times 10^8$ $M_\odot$. This is similar to the amount inferred in the Fornax A features (Mackie & Fabbiano 1998), and is also similar to the mass of HI found in the southeastern tail of NGC 4410A+B. Perhaps in the bridge the atomic gas has been converted to hot ionized gas, but in the southeastern tail the gas has remained atomic. Further observations are needed to resolve the question of whether the extended X-ray emission near NGC 4410A is due to intracluster gas or gas affiliated with the bridge.

4.2. *A Jet-Intracluster Medium Encounter?*

Stocke & Burns (1987) suggest that the peculiar radio structure of NGC 4410A is due to motion through an intracluster medium. The new ROSAT data provides stronger constraints on this hypothesis while not ruling it out completely. As noted above, NGC 4410A+B is detected in X-rays, however, this emission is confined to the immediate vicinity of the galaxies and a tail-like feature extending to the east (Figure 4b). It is possible that this 'tail' is associated with the stellar bridge and is not truly intracluster gas (Section 4.1). Excluding this feature, the ROSAT PSPC 3σ upper limit to the diffuse X-ray emission from the group is 4×10^{-7} counts s^{-1} arcsec^{-2}, which corresponds to 5×10^{-18} erg s^{-1} cm^{-2} arcsec^{-2}, assuming a 1 keV Raymond-Smith plasma and $N_H = 1.7 \times 10^{20}$ cm^{-2}. This gives an average density of the intracluster medium in the group of $\leq 6 \times 10^{-4}$ cm^{-3}, assuming standard cooling functions (McKee & Cowie 1977; McCray 1987). This is lower than the densities inferred in many rich clusters and compact groups (e.g., Jones & Forman 1984; Pildis et al. 1995), but consistent with those found in some poor clusters (Doe et al. 1995), some of which contain 'head-tail' radio sources.

This upper limit on the intracluster gas density is not inconsistent with pressure confinement of the radio lobes by an ambient medium. Using the method described by O'Dea & Owen (1987), we calculated the minimum pressure P_{min} in the southeastern radio lobe of NGC 4410A+B, assuming a spectral index of $\alpha \sim 1$ ($F_\nu \propto \nu^{-\alpha}$), lower and upper frequency cutoffs of 10 MHz and 10 GHz respectively, a volume filling factor of 1, and equal proton and electron energies. Using the volume emissivity given in Hummel et al. (1986), $P_{min} = 4.6 \times 10^{-13}$ dynes cm^{-2} for the diffuse emission in the lobe. If this diffuse emission is in pressure equilibrium with the surrounding intracluster medium, $\rho_{ICM} \sim 2 \times 10^{-4}$ cm^{-3} (calculated as in Stocke & Burns 1987), in agreement with the ROSAT upper limit.

This upper limit on the amount of diffuse hot gas in the group can be compared with the virial mass of the group. The luminosity-weighted velocity dispersion in the NGC 4410 group (from Table 1a) is 225 km s^{-1}. Using an effective radius of $\sim 5'$ (140 kpc), the virial mass is 5.1×10^{12} $M_\odot$. This gives a M/L_B ratio of ~ 30 $M_\odot/L_\odot$ for the group, typical of poor groups (e.g., Mulchaey et al. 1996). From the ROSAT map, we infer an upper limit to the mass of hot gas in this group of $\leq 2 \times 10^{11}$ $M_\odot$, $\leq$4% of the virial mass, consistent with the 3– 6% found for other groups (Pildis et al. 1995; Mulchaey et al. 1996).

An intracluster medium density of $\sim 10^{-4}$ cm^{-3} is sufficient to produce a 'head-tail' radio structure, provided the velocity of the galaxy with respect to the intracluster medium is high enough or the density in the jet is low enough (Stocke & Burns 1987; Venkatesan et al. 1994; Doe et al. 1995). For a non-relativistic jet, the radius of curvature of the jet is $R = r_j \rho_j {v_j}^2 / \rho_{ICM} {v_g}^2$ (Burns 1981; Eilek et al. 1984), where r_j is the radius of the jet, ρ_j and ρ_{ICM} are the densities of the jet and the intracluster medium respectively, v_j is the velocity of the jet, and v_g is the velocity of the galaxy with respect to the intracluster gas. This equation shows that a small radius of curvature can be achieved with a sufficiently large v_g or low ρ_j, even if the intracluster medium density is low.

To test whether this condition holds in NGC 4410, we must estimate the parameters of the jet. Assuming that the distorted southeastern lobe is indeed a gradually curving jet, we estimate a radius of curvature R of $\sim 1.'5$ (40 kpc) from the Hummel et al. (1986) maps. To estimate the physical conditions in this jet, we assume that the observed radio luminosity of the lobe L_r is powered by the bulk kinetic energy in the jet, so $L_r \sim \pi \rho_j {r_j}^2 {v_j}^3 \epsilon / 2$, where ϵ is the efficiency of the conversion (Burns 1981; Eilek et al. 1984). The radio luminosity of the southeastern lobe L_r is 1.3×10^{41} erg s^{-1} (Hummel et al. 1986). Assuming that the prominent ridge extending southeast from the nucleus (Hummel et al. 1986) is the jet gives $r_j \sim 10''$ (5 kpc). Using these values and assuming $v_j \leq 0.2c$ and $\epsilon \leq 0.01$ (O'Dea 1985; O'Donoghue, Eilek, & Owen 1993; Borne & Colina 1993), we find that the internal ram pressure in the jet is $\rho_j {v_j}^2 \geq 4 \times 10^{-12}$ dynes cm^{-2}. For comparison, using the assumptions given above and the Hummel et al. (1986) volume emissivity, the minimum pressure P_{min} in the more northern of the radio knots in the southeastern lobe is 1.3×10^{-12} dynes cm^{-2}, consistent with this estimate.

Using our estimate of the internal ram pressure in the NGC 4410 jet, we find that the velocity of the galaxy relative to the intracluster medium v_g must be greater than 220 km s^{-1} to have caused the observed bending of the radio lobe. A more moderate jet velocity of $\sim 10^4$ km s^{-1} (e.g., Borne & Colina 1993) gives a lower limit of $v_g \geq 660$ km s^{-1}. The radial velocity of NGC 4410A, 7440 km s^{-1}, is close to the luminosity-weighted mean velocity of the group, 7355 km s^{-1}. Therefore, if the distortion of the lobe was caused by ram pressure bending by an intracluster medium at rest with respect to the group, much of this motion must be in the plane of the sky. Optically, NGC 4410A is the most luminous galaxy in the group, providing 1/4 of its total blue luminosity. It has an absolute blue magnitude of –21.1, approaching that of M87. This argues against the idea that NGC 4410A has a large motion relative to the group as a whole. Therefore, if the group is virialized, then the distortion of the radio lobe may not have been caused by an interaction with an intracluster medium.

4.3. *A Jet-Interstellar Medium Encounter?*

The HI tail to the southeast of NGC 4410A+B, overlapping with the bright southeastern radio lobe, suggests an intriguing alternative explanation for the peculiar radio morphology in this system: perhaps it is not due to an interaction with an intracluster medium, as in classical models of head-tail systems, but instead is due to an interaction with the interstellar medium in the system. Interactions between jets and interstellar gas disturbed by a gravitational encounter or merger between galaxies have been suggested for a number of systems, including 4C 29.30 (van Breugel et al. 1986) and Centaurus A (de Young 1981). Although it is possible that the southeastern tidal tail and the radio lobe of 4410A+B are merely superposed structures, extending out from the pair of galaxies in different directions, the apparent abrupt bend in the radio lobe (Hummel et al. 1986) suggests that they are interacting, as does the discontinuity in the HI velocity structure of this tail (Figure 3).

It is uncertain at present if there is sufficient interstellar matter in the southeastern tail to account for the bending of the lobe, because of the lack of information about the properties of the jet and the timescale of the impact. A gas cloud of mass M_c impacted by a jet has an acceleration a_c given by $M_c a_c = \rho_j v_j^2 \pi r_j^2$ (Eilek et al. 1984). Using the relationship provided above for the jet parameters in terms of the radio luminosity L_r gives $M_c \sim 2 L_r t_c / \epsilon v_j v_c$, assuming the cloud has been accelerated to a velocity v_c over a period t_c. Assuming $v_c \sim 240$ km s^{-1} (from Figure 3; the maximum radial velocity difference between the HI in the tail and the nucleus) and $\epsilon \sim 0.01$, $M_c \sim 3 \times 10^6$

$(60000/v_j \text{ km s}^{-1})/(t_c/10^6 \text{ years}) \text{ M}_\odot$. For comparison, the mass of HI in this tail is 3×10^8 $\text{M}_\odot$ (Section 3.1.2). Therefore, if the timescale is short and/or the jet velocity is high, there is sufficient interstellar gas to bend the jet. The timescale t_c is uncertain, but it must be less than the age of the radio source. Therefore $t_c \leq D_{\textit{northern lobe}}/v_j$, where the $D_{\textit{northern lobe}}$ is the spatial extent of the northern lobe (180 kpc). As noted above, the jet velocity v_j is uncertain, but is probably less than 0.2c (e.g., O'Dea 1985; O'Donoghue, Eilek, & Owen 1993; Borne & Colina 1993). If v_j is close to this upper limit, then $t_c \leq 3 \times 10^6$ years and the required mass $M_c \leq 9 \times 10^6$ $\text{M}_\odot$, less than the amount of interstellar gas in the tail. If v_j is small and the timescale of impact is long, however, the gas in the tail may not be sufficient to bend the radio structure.

A related question is whether the gas in the tail is able to bend the jet to the observed angle ($\sim$70°; Hummel et al. 1986). This angle is larger than the bends in some radio structures where jet-cloud interactions are thought to have occurred (van Breugel et al. 1985a, 1986; Stocke et al. 1985). However, there are a few other examples of radio lobes bent at large angles (Stocke et al. 1985; Borne & Colina 1993), so NGC 4410 is not unique. There have been a number of theoretical studies of jet bending in the literature (e.g., Valtaoja 1984; Fiedler & Henriksen 1984; William & Gull 1985; Stocke et al. 1985; Lonsdale & Barthel 1986; Borne & Colina 1993). Of these models, the one that may be the most relevant for NGC 4410 is the Borne & Colina (1993) simulation of the 70° bend in the eastern 3C 278 radio lobe from ram pressure due to the interstellar medium in a companion, caused by the companion's motion relative to the radio jet. Using estimated orbital parameters of the host galaxy NGC 4782 and its companion NGC 4783, Borne & Colina (1993) successfully reproduced the observed bending of the 3C 278 jet. Their model demonstrates that ram pressure due to the interstellar matter in a companion moving past a radio galaxy is indeed capable of bending a jet to large angles.

4.4. *A Group-Group Merger?*

If the group is dynamically young, the argument given in Section 4.2 against ram pressure bending by the intracluster medium does not hold (e.g., Venkatesan et al. 1994; Doe et al. 1995). It is possible that there is a large-scale motion of the group relative to an intracluster medium, perhaps due to the merging of two groups. Bliton et al. (1998) compared the radial velocities of a sample of 23 head-tail galaxies in clusters with the cluster mean velocities and dispersions, and concluded that the relative velocities are too small to account for the distortion of the radio lobes. They suggested that these systems are undergoing cluster-cluster mergers, which are driving bulk flows of the intracluster medium. Such a process may be occurring in the NGC 4410 group; two of the galaxies in the group, NGC 4410D and VCC 822, have radial velocities that differ from the mean by 500 km s^{-1}. If the extended X-ray emission noted earlier is indeed intracluster gas rather than material associated with the bridge, then the intracluster gas is quite inhomogeneous, supporting the idea of a group-group merger. To test this possibility, higher sensitivity X-ray data of the NGC 4410 group would be useful.

It is possible that the on-going interaction between NGC 4410A and NGC 4410B has been driven by the merger of two groups of galaxies, and the disturbance of the radio structure was caused by an interaction with both the interstellar and the intracluster medium, both having been perturbed by the encounter. The radio morphology of NGC 4410 resembles that of the peculiar system 3C 442 in some respects. Comins & Owen (1991) suggest that the distorted radio lobes and prominent ridges found in 3C 442 were created during the merger of two clusters. The host galaxy of 3C 442 is currently merging with a companion galaxy; if this galaxy-galaxy merger was driven by a cluster-cluster merger, in addition to perturbed interstellar matter, there may be disturbed intracluster matter which could be disrupting the radio lobes. Based upon the observation of a relatively constant 6 to 20 cm spectral index of $\alpha \sim 1.1$ along the 3C 442 lobe, Comins & Owen (1991) suggest that electrons in the 3C 442 lobes may have been re-accelerated by turbulence from the interaction. The southeast lobe of NGC 4410 also has a relatively constant spectral index of $\alpha \sim 1.0$ (Hummel et al. 1986), arguing for re-acceleration in that structure as well. Whether this re-acceleration and the observed distortion of the radio lobe were caused by an encounter with the interstellar or intracluster matter is as yet uncertain. However, the existence of a considerable amount of interstellar matter in the NGC 4410 system, along with the non-detection of diffuse intracluster medium in the group, argues that interstellar gas played a major role in the shaping of the radio structure in this system.

5. CONCLUSIONS

Using the VLA and the NRAO 12m telescope, we mapped the radio continuum emission, the 21 cm HI line, and the 2.6mm CO line in the peculiar interacting galaxy pair NGC 4410A+B. We discovered a low surface brightness radio lobe extending 6.′2 (180 kpc) to the northwest of the pair, opposite the bright southeastern lobe seen in previous observations. The existence of this second lobe confirms that NGC 4410A is a double-lobed radio galaxy, albeit with a severely distorted structure.

We have detected both HI and CO in this system, yielding $M_{HI} \sim 10^9$ $\text{M}_\odot$ and $M_{H_2} \sim 4 \times 10^9$ $\text{M}_\odot$. The molecular gas is concentrated in the radio galaxy NGC 4410A while the HI is more extended. There is a 3×10^8 $\text{M}_\odot$ HI tail extending 1.′7 (50 kpc) to the southeast of the pair, coincident with an optical tail. This HI tail overlaps part of the southeastern radio lobe. Comparison with a recent ROSAT PSPC X-ray map of this system shows an anti-coincidence of the HI with an X-ray feature that extends due east from NGC 4410A. This X-ray structure contains 3–8 $\times 10^8$ $\text{M}_\odot$ of hot gas and appears to be aligned with a stellar bridge connecting the pair to a third galaxy. It is not clear at present whether the extended X-ray emitting gas is intracluster material or shocked gas associated with the bridge.

We suggest that the distortion of the radio structure was caused by ram pressure from the interstellar medium in the system, due to the motion of the interstellar matter relative to the radio source during the gravitational interaction of NGC 4410A with NGC 4410B. An alternative possibility is that the peculiar radio structure may be due to motion through an intragroup medium, however, the small radial velocity of NGC 4410A relative to the group and the lack of diffuse X-ray emission in the group makes this scenario somewhat less likely, unless the group is not virialized or is merging with another group.

In addition to NGC 4410A+B, we detected HI in six other galaxies in the NGC 4410 group. The total HI in the group is 1.4×10^{10} $\text{M}_\odot$, 80% of which arises from four galaxies in the outer group. Three of these galaxies (VCC 831, VCC 822, and VCC 847) are spirals with M_{HI}/L_B ratios typical of field galaxies, while FGC 170A appears to be a gas-rich dwarf galaxy. In

the inner group, the SBa galaxy NGC 4410D (VCC 934) was detected in both HI and CO and has a 2×10^8 $M_\odot$ HI tail extending $1'$ (28 kpc) towards the nearby disk galaxy NGC 4410F. NGC 4410F was also seen in HI but not in CO. The galaxies in the inner group appear to be somewhat deficient in HI compared to their blue luminosities, suggesting phase changes driven by galaxy-galaxy or galaxy-intracluster medium encounters.

We would like to thank Liese van Zee, Michael Rupen, and Jason Wurnig for their help in planning for and reducing the VLA observations. We also appreciate the help of the telescope operators and staff of the NRAO 12m telescope in obtaining the CO data. We thank the referee Jacqueline van Gorkom, Frazer Owen, Curt Struck, Daniel Tschöke, and Bev Wills for helpful comments on this paper, and Daniel Tschöke and Megan Donahue for providing us with copies of their X-ray and optical maps. This research has made use of the NASA/IPAC Extragalactic Database (NED) which is operated by the Jet Propulsion Laboratory under contract with NASA. We are pleased to acknowledge partial funding for this project from a NASA grant administrated by the American Astronomical Society. Partial support was also provided from NASA grant AR-08374.01-97A from the Space Telescope Science Institute, which is operated by AURA, Inc., under NASA contract NAS 5-26555.

REFERENCES

Batuski, D. J., Hanisch, R. J., & Burns, J. O. 1992, AJ, 103, 1077
Baum, S. A., Heckman, T., Bridle, A., van Breugel, W., & Miley, G. 1988, ApJS, 68, 643
Bieging, J. H., & Biermann, P. 1983, AJ, 88, 161
Binggeli, B., Sandage, A., & Tammann, G. A. 1985, AJ, 90, 1681
Bliton, M., Rizza, E., Burns, J. O., Owen, F. N., & Ledlow, M. J. 1998, MNRAS, 301, 609
Bloemen, J. B. G. M., et al. 1986, A&A, 154, 25
Briggs, D. 1995, Ph.D. Thesis, New Mexico Institute of Mining & Technology.
Burns, J. O. 1981, MNRAS, 195, 523
Borne, K. D., & Colina, L. 1993, ApJ, 416, 157
Bregman, J. N., Schulman, E., & Tomasaka, K. 1995, ApJ, 439, 155
Colina, L., & de Juan, L. 1995, ApJ, 448, 548
Comins, N. F., & Owen, F. N. 1991, ApJ, 382, 108
Condon, J. J., Frayer, D. T., & Broderick, J. J. 1991, AJ, 101, 362
Dahlem, M., Weaver, K. A., & Heckman, T. M. 1998, ApJS, 118, 401
De Young, D. S. 1981, Nature, 293, 43
De Vaucouleurs, G., De Vaucouleurs, A., Corwin, Jr., H. G., Buta, R. J., Paturel, G., & Fouque, P. 1991, Third Reference Catalogue of Bright Galaxies, Version 3.9 (RC3)
Dickey, J. M., & Lockman, F. J. 1990, ARAA, 28, 215
Doe, S. M., Ledlow, M. J., Burns, J. O., & White, R. A. 1995, AJ, 110, 46
Donahue, M., et al. 2000, in preparation
Dressel, L. L., Bania, T. M., & O'Connell, R. W. 1982, ApJ, 259, 55
Duc, P.-A., Brinks, E., Wink, J. E., & Mirabel, I. F. 1997, A&A, 326, 537
Eilek, J. A., Burns, J. O., O'Dea, C. P., & Owen, F. N. 1984, ApJ, 278, 37
Fabbiano, G. 1988, ApJ, 330, 672
Faber, S. M., & Gallagher, J. S. 1979, ARAA, 17, 135
Fiedler, R., & Henriksen, R. N. 1984, ApJ, 281, 554
Graham, J. A. 1998, ApJ, 502, 245
Hansen, L., Norgaard-Nielsen, H. U., & Jorgensen, H. E. 1987, A&AS, 71, 465
Harris, D. E., Leighly, K. M., & Leahy, J. P. 1998, ApJ, 499, L149
Heckman, T. M., Smith, E. P., Baum, S. A., van Breugel, W. J. M., Miley, G. K., Illingworth, G. D., Bothun, G. D., & Balick, B. 1986, ApJ, 311, 526
Heckman, T. M., Dahlem, M., Eales, S. A., Fabbiano, G., & Weaver, K. 1996, ApJ, 457, 616
Hes, R., Barthel, P. D., & Fosbury, R. A. E. 1996, A&A, 313, 423
Hibbard, J. E., Guhathakurta, P., van Gorkom, J. H., & Schweizer, F. 1994, AJ, 107, 67
Hibbard, J. E., & van Gorkom, J. H. 1996, AJ, 111, 655
Hoffman, G. L., Lewis, B. M., Helou, G., Salpeter, E. E., & Williams, H. L. 1989, ApJS, 69, 65
Holtzman, J. A., et al. 1992, AJ, 103, 691
Hummel, E., Kotanyi, C. G., & van Gorkom, J. H. 1986, A&A, 155, 161
Jenkins, C. R. 1983, MNRAS, 205, 1321
Jones, C., & Forman, W. 1984, ApJ, 276, 38
Kenney, J. D. P., & Young, J. S. 1989, ApJ, 344, 171
Kotanyi, C. G. 1980, A&AS, 41, 421
Ledlow, M. J., & Owen, F. N. 1995, AJ, 110, 1959
Lees, J. F. 1992, Ph. D. Thesis, Princeton University.
Lilly, S. J., & Prestage, R. M. 1987, MNRAS, 225, 531
Lonsdale, C. J., & Barthel, P. D. 1986, AJ, 92, 12
Lonsdale, C. J., Helou, G., Good, J. C., & Rice, W. 1985, Catalogued Galaxies and Quasars Observed in the IRAS Survey (Pasadena: Jet Propulsion Laboratory)
Mackie, G., & Fabbiano, G. 1998, ApJ, 115, 514
Malkan, M. A., Gorjian, V., & Tam, R. 1998, ApJS, 117, 25
Mazzarella, J. M., & Boroson, T. A. 1993, ApJS, 85, 27
Mazzarella, J. M., Bothun, G. D., & Boroson, T. A. 1991, AJ, 101, 2034
Mazzarella, J. M., Graham, J. R., Sanders, D. B., & Djorgovski, S. 1993, ApJ, 409, 170
McCarthy, P. J., Spinrad, H., & van Breugel, W. 1995, ApJS, 99, 27
McCray, R. 1987, in Spectroscopy of Astrophysical Plasmas, ed. A. Dalgarno and D. Layzer (Cambridge University Press: New York, NY), p. 260
McKee, C. F., & Cowie, L. L. 1977, ApJ, 215, 213
Miley, G. K., Perola, G. C., van der Kruit, P. C., & van der Laan, H. 1972, Nature, 237, 269
Mirabel, I. F., Sanders, D. B., & Kazès, I. 1989, ApJ, 340, L9
Mirabel, I. F., Dottori, H., & Lutz, D. 1992, A&A, 256, L19
Morganti, R., Ulrich, M.-H., & Tadhunter, C. N. 1992, MNRAS, 254, 546
Mukai, K. 1993, Legacy 3, 21 (http://rosat.gsfc.nasa.gov/Tools/w3pimms.html)
Mulchaey, J. S., Davis, D. S., Mushotzky, R. F., & Burstein, D. 1996, ApJ, 456, 80
O'Dea, C. P. 1985, ApJ, 295, 80
O'Dea, C. P., & Owen, F. N. 1985, AJ, 90, 954
O'Dea, C. P., & Owen, F. N. 1987, ApJ, 316, 95
O'Donoghue, A. A., Eilek, J. A., & Owen, F. N. 1993, ApJ, 408, 428
Owen, F. N., & White, R. A. 1991, MNRAS, 249, 164
Pildis, R. A., Bregman, J. N., & Evrard, A. E. 1995, ApJ, 443, 514
Raimon, E., Faber, S. M., Gallagher, J. S., & Knapp, G. R. 1981, ApJ, 246, 708
Read, A. M., Ponman, T. J., & Strickland, D. K. 1997, MNRAS, 286, 626
Read, A. M., Ponman, T. J., & Wolstencroft, R. D. 1995, MNRAS, 277, 397
Read, A. M., & Ponman, T. J. 1998, MNRAS, 297, 143
Rice, W., Lonsdale, C. J., Soifer, B. T., Neugebauer, G., Kopan, E. L., Lloyd, L. A., de Jong, T., & Habing, H. J. 1988, ApJS, 68, 91
Schiminovich, D., van Gorkom, J. H., van der Hulst, J. M., & Kasow, S. 1994, ApJ, 423, L101
Smith, B. J. 1991, ApJ, 378, 39
Smith, B. J., & Harvey, P. M. 1996, ApJ, 468, 139
Simkin, S. M., & Callcut, J. 1996, in Extragalactic Radio Sources, IAU Symp. 175, ed. R. Ekers, C. Fanti, & L. Padrielli ((Dordrecht: Boston), p. 183
Stocke, J. T., & Burns, J. O. 1987, ApJ, 319, 671
Stocke, J. T., Burns, J. O., & Christiansen, W. A. 1985, ApJ, 299, 799
Tschöke, D., Hensler, G., & Junkes, N. 1999, A&A, 343, 373
Toomre, A. 1977, in Evolution of Galaxies and Stellar Populations, eds. B. M. Tinsley and R. B. Larson (New Haven, Yale University Observatory), p. 401
Valtaoja, E. 1984, A&A, 140, 148
Van Breugel, W. J. M., & Dey, A. 1993, ApJ, 414, 563
Van Breugel, W., Miley, G., Heckman, T., Butcher, H., & Bridle, A. 1985a, ApJ, 290, 496
Van Breugel, W. J. M., Filippenko, A. V., Heckman, T., & Miley, G. 1985b, ApJ, 293, 83
Van Breugel, W. J. M., Heckman, T., Butcher, H., & Miley, G. 1984, ApJ, 277, 82
Van Breugel, W. J. M., Heckman, T. M., Miley, G. K., & Filippenko, A. V. 1986, ApJ, 311, 58
Van Gorkom, J. H., Knapp, G. R., Ekers, R. D., Ekers, D. D., Laing, R. A., & Polk, K. S. 1989, AJ, 97, 708
Van Gorkom, J. H., Knapp, G. R., Raimond, E., Faber, S. M., & Gallagher, J. S. 1986, AJ, 91, 791
Van Gorkom, J. H., van der Hulst, J. M., Haschick, A. D., & Tubbs, A. D. 1990, AJ, 99, 1781
Venkatesan, T. C. A., Batuski, D. J., Hanisch, R. J., & Burns, J. O. 1994, ApJ, 436, 67
Véron-Cetty, M.-P., Woltjer, L., Ekers, R. D., & Staverley-Smith, L. 1995, A&A, 297, L79
William, A. G., & Gull, S. F. 1985, Nature, 313, 34
Zirbel, E. L. 1996, ApJ, 473, 713

Captions

FIG. 1.— a) A 500 second archival Hubble Space Telescope (HST) WFPC2 image of NGC 4410, taken with the broadband red F606W filter. These data were originally obtained as part of the Malkan et al. (1998) HST survey of active galaxies, and have previously been presented by Tschöke et al. (1999). b) A $1\farcm1 \times 0\farcm9$ field of view narrowband red continuum image of NGC 4410A+B, obtained with the Kitt Peak 2.1m telescope (Donahue et al. 2000). NGC 4410A is the more western galaxy. c) The inner $6\farcm4 \times 4\farcm9$ of the NGC 4410 group, as seen in a deep R band image from the Southeastern Association for Research in Astronomy (SARA) telescope (from Donahue et al. 2000). The five major members are labeled. d) The Digitized Sky Survey image of the NGC 4410 group. The 23 known galaxies in the field are marked, as well as four anonymous galaxies (see Tables 1a – c). Twelve of these galaxies are part of the NGC 4410 group, two (NGC 4411 and NGC 4411B) belong to the foreground Virgo Cluster, and four to a background group. The rest of the galaxies have no published redshifts.

FIG. 2.— Our naturally-weighted 20 cm continuum map of the NGC 4410 field (contours), superposed on the Digitized Sky Survey map (greyscale). The first contour is 0.75 mJy beam^{-1} and the contour intervals increase by multiples of $\sqrt{2}$. The beamsize is $59\farcs38 \times 54\farcs67$. For clarity, this map has not been corrected for primary beam attenuation. The noise level in the inner portion of the map is 0.17 mJy beam^{-1}.

FIG. 3.— The naturally-weighted HI channel maps of the inner portion of the NGC 4410 group (contours), superposed on the optical DSS map (greyscale). The contour levels are -2σ, 2σ, 4σ, 6σ, 8σ, and 10σ, where 1σ = 0.21 mJy beam^{-1}. The HI beamsize in this map is $59\farcs38 \times 54\farcs67$.

FIG. 4.— a) The naturally-weighted HI intensity map of the inner portion of the NGC 4410 group (contours), superposed on the R band image from Donahue et al. (2000) (greyscale). The first contour is 2×10^{19} cm^{-2}; the contour interval is 10^{19} cm^{-2}. The HI beamsize is $59\farcs38 \times 54\farcs67$. b) The HI intensity map (blue contours), the radio continuum map (white contours), and the ROSAT PSPC X-ray map (yellow contours), all superposed on the R band image (greyscale). The first radio continuum contour is 0.75 mJy beam^{-1} and the contour intervals increase by multiples of $\sqrt{2}$. The contour levels on the X-ray maps are 3σ, 4σ, 7σ, 12σ, 19σ, 28σ, 39σ, and 52σ above the background, where the background is 1.4×10^{-2} counts arcsec^{-2} and the rms noise is 3×10^{-3} counts arcsec^{-2}. The spatial resolution of the PSPC map is $25''$, and the total integration time with ROSAT was 23.4 ksec.

FIG. 5.— A larger field of view display of the naturally-weighted HI intensity map (contours), showing the entire NGC 4410 group. This image is superposed on the optical DSS image (greyscale). The first contour is 3×10^{19} cm^{-2} and the contour interval is 6×10^{19} cm^{-2}. The increased noise at the edges of the field is due to the primary beam correction. The beamsize is $59\farcs38 \times 54\farcs67$.

FIG. 6.— a-b) The total 21 cm HI spectra for the detected galaxies in the NGC 4410 group. These have been corrected for primary beam attenuation.

FIG. 7.— The CO spectra for the observed galaxies in the NGC 4410 group. For displaying purposes, these spectra have been smoothed by a 36 km s^{-1} boxcar and then resampled at 21 km s^{-1} spacing.

FIG. 8.— a-d) The naturally-weighted HI MOM1 maps (contours) for the four detected galaxies in the outer part of the NGC 4410 group, superposed on the optical DSS images (greyscale). The contour intervals are 10 km s^{-1}. Several contours are labeled, in units of km s^{-1}.

Table 1a
Galaxies in the inner 30′ Diameter of the NGC 4410 Group[a]

Name	Position						Type	m_B	Velocity
	R.A. (1950)			Dec. (1950)					(km/s)
NGC 4410A[b]	12	23	55.7	9	17	47	Sab Pec?	13.8	7440[c]
NGC 4410B[b]	12	23	57.2	9	17	46	S0? Pec	15.0	7500[c]
NGC 4410C (IC 790)	12	24	2.9	9	18	43	S0?	15.5	7525
NGC 4410D (VCC 934)	12	24	11.7	9	19	31	SBa(s)	14.8	6938
NGC 4410E (LEDA 094212)	12	23	59.1	9	23	59	S[d]	16.0	7355
NGC 4410F[b]	12	24	8.2	9	17	30		16[d]	7206[e]
NGC 4410H (VCC 961)	12	24	26.6	9	14	7	SB0	15.0	7342
VCC 822	12	23	8.0	9	11	28	SBc	15.0	6898
VCC 831	12	23	11.0	9	18	12	Sc	15.0	7507
VCC 847	12	23	19.0	9	12	2	SBc	14.9	7556
FGC 170A	12	24	34.0	9	29	54	S[d]	17[d]	7620[f]
NGC 4410K (1224+0919)	12	24	56.7	9	19	11		15[d]	7458

[a]All information from the NASA/IPAC Extragalactic Database (NED), unless otherwise noted. The nomenclature used for NGC 4410A–H, K is from Stocke & Burns (1987). The velocities are optical heliocentric values.
[b]Position measured from the Digitized Sky Survey (DSS) image.
[c]Optical velocity from Donahue et al. (2000).
[d]Estimated from the Digitized Sky Survey (DSS) image.
[e]Optical velocity from Stocke & Burns (1987), converted from v_{LSR} to v_{helio} as in the RC3.
[f]HI velocity from this work.

Table 1b
Foreground and Background Objects in the NGC 4410 Field[a]

Name	Position						Type	m_B	Velocity
	R.A. (1950)			Dec. (1950)					(km/s)
NGC 4411[b]	12	23	56.6	9	8	53	SB(rs)c	13.4	1281
NGC 4411B[b]	12	24	14.7	9	9	41	SAB(s)cd	12.9	1270
LEDA 094219	12	24	53.0	9	13	38	S[c]	17.3	26372
NGC 4410I (Abell 1541)	12	24	15.6	9	14	17		16[c]	25828
NGC 4410G[d] (LEDA 094214)	12	24	25.0	9	17	41		17.2	27462
NGC 4410J[d]	12	24	31.3	9	22	19	S[c]	16[c]	25066[e]

[a]All information from the NASA Extragalactic Database (NED), unless otherwise noted. The nomenclature used for NGC 4410G, I, and J is from Stocke & Burns (1987).
[b]Member of the Virgo Cluster (Binggeli et al. 1985).
[c]Estimated from the Digitized Sky Survey (DSS) image.
[d] Position measured from the DSS.
[e]Optical velocity from Stocke & Burns (1987), converted from v_{LSR} to v_{helio} as in the RC3.

Table 1c
Galaxies in the NGC 4410 Field with Unknown Velocities[a]

Name	Position						Type	m_B
	R.A. (1950)			Dec. (1950)				
VCC 869[b]	12	23	33.3	9	14	39	ImV or dE0	15.0
VCC 914[b]	12	24	1.2	9	16	12	dE,N	19.0
VCC 933[b]	12	24	11.4	9	6	0	dE2,N	16.6
VCC 902[b]	12	23	55.2	9	4	24	dE0	18.3
VCC 976[b]	12	24	39.0	9	6	54	dE4	18.0
ANON 1[c]	12	22	57.6	9	20	55.6		16[d]
ANON 2[c]	12	23	12.6	9	16	27		16.5[d]
ANON 3[c]	12	24	0.3	9	19	36		17[d]
ANON 4[c]	12	24	36.8	9	27	38		16[d]

[a]All information from the NASA Extragalactic Database (NED), unless otherwise noted.
[b]Based on optical morphology, Binggeli et al. (1985) conclude this is probably a member of the Virgo Cluster.
[c]Position measured from the Digitized Sky Survey (DSS) image.
[d]Estimated from the Digitized Sky Survey (DSS) image.

Table 2
VLA 21 cm HI Results for the NGC 4410 Group

Name	HI Line Flux (Jy km s^{-1})	Central Velocity (km s^{-1})	ΔV (FWHM) (km s^{-1})
NGC 4410A+B	0.55 ± 0.16	7350	260
NGC 4410C	≤ 0.08[a]		
NGC 4410D	0.22 ± 0.04	6960,7380	90,90
NGC 4410E	≤ 0.10[a]		
NGC 4410F	0.17 ± 0.05	7180	90
NGC 4410H	≤ 0.09[a]		
VCC 822	1.63 ± 0.13	6900[c]	200[c]
VCC 831	0.74 ± 0.11	7430	220
VCC 847	1.14 ± 0.07	7550[b]	250[b]
FGC 170A	1.21 ± 0.13	7620[b]	160[b]
1224+0919	≤ 0.16[a]		

[a]Assuming a line width of $\leq$600 km s^{-1} and a $\leq 30''$ (14 kpc) diameter HI disk.
[b]Near the edge of the observed bandpass. Some high velocity gas may have been missed.
[c]Near the edge of the observed bandpass. Some low velocity gas may have been missed.

Table 3
NRAO 12m CO (1-0) Results for the NGC 4410 System

Name	T_R^* (rms) (mK)	I_{CO}[a] (K km s^{-1})	Velocity (km s^{-1})	ΔV[b] (km s^{-1})
NGC 4410A	1.5	1.12 ± 0.09	7140,7300,7565	600
NGC 4410B	1.6	≤ 0.30[c]		
NGC 4410A+B Tail[d]	1.5	≤ 0.18[e]		
NGC 4410C	2.8	≤ 0.47[f]		
NGC 4410D	2.1	0.24 ± 0.08	6960	150
NGC 4410F	2.1	≤ 0.14[g]		

[a] Statistical uncertainties only. Upper limits are 3σ.
[b] Full width half maximum line widths (FWHM).
[c] Assuming a line width of $\leq$800 km s^{-1}.
[d] Centered at $12^h\ 23^m\ 58.3^s\ 9^\circ\ 17'\ 11.''5$ (1950).
[e] Using the HI line width of 300 km s^{-1} (Figure 3).
[f] Assuming a line width of $\leq$600 km s^{-1}.
[g] Using the FWHM HI line width of 90 km s^{-1} (Table 2)

Table 4
Global Parameters for the Galaxies in the NGC 4410 Group

Name	M_{HI} ($M_\odot$)	M_{H_2}[a] ($M_\odot$)	L_B[b] ($L_\odot$)	M_{HI}/L_B ($M_\odot/L_\odot$)	M_{H_2}/M_{HI}
NGC 4410A+B	1.3×10^9	3.9×10^9	5.7×10^{10}	0.022	3.0
NGC 4410C	$\leq 1.8 \times 10^8$	$\leq 1.7 \times 10^9$	9.0×10^9	$\leq$0.020	
NGC 4410D	5.0×10^8	8.4×10^8	1.7×10^{10}	0.029	1.7
NGC 4410E	$\leq 2.2 \times 10^8$		5.6×10^9	$\leq$0.039	
NGC 4410F	3.8×10^8	$\leq 5.0 \times 10^8$	5.6×10^9	0.068	$\leq$1.3
NGC 4410H	$\leq 2.0 \times 10^8$		1.4×10^{10}	$\leq$0.014	
VCC 822	3.6×10^9		1.4×10^{10}	0.26	
VCC 831	1.7×10^9		1.4×10^{10}	0.12	
VCC 847	2.5×10^9		1.6×10^{10}	0.16	
FGC 170A	2.6×10^9		2.2×10^9	1.20	
1224+0919	$\leq 3.6 \times 10^8$		1.4×10^{10}	$\leq$0.026	

[a] Calculated assuming the standard Galactic I_{CO}/N_{H_2} ratio ($M_{H_2} = 1.1 \times 10^4\ D^2 \int S_V dV$, where D is the distance in Mpc; Bloemen et al. 1986), H_o = 75 km s^{-1} Mpc^{-1}, and assuming a point source (η_c = 1) and 34 Jy K^{-1} for the 12m telescope.
[b] Assuming $M_{B_\odot}$ = 5.48.

This figure "f1a.jpg" is available in "jpg" format from:

http://arXiv.org/ps/astro-ph/0005093

This figure "f1b.jpg" is available in "jpg" format from:

http://arXiv.org/ps/astro-ph/0005093

This figure "f1c.jpg" is available in "jpg" format from:

http://arXiv.org/ps/astro-ph/0005093

This figure "f1d.jpg" is available in "jpg" format from:

http://arXiv.org/ps/astro-ph/0005093

This figure "f2.jpg" is available in "jpg" format from:

http://arXiv.org/ps/astro-ph/0005093

This figure "f3.jpg" is available in "jpg" format from:

http://arXiv.org/ps/astro-ph/0005093

This figure "f4a.gif" is available in "gif" format from:

http://arXiv.org/ps/astro-ph/0005093

This figure "f4b.gif" is available in "gif" format from:

http://arXiv.org/ps/astro-ph/0005093

This figure "f5.jpg" is available in "jpg" format from:

http://arXiv.org/ps/astro-ph/0005093

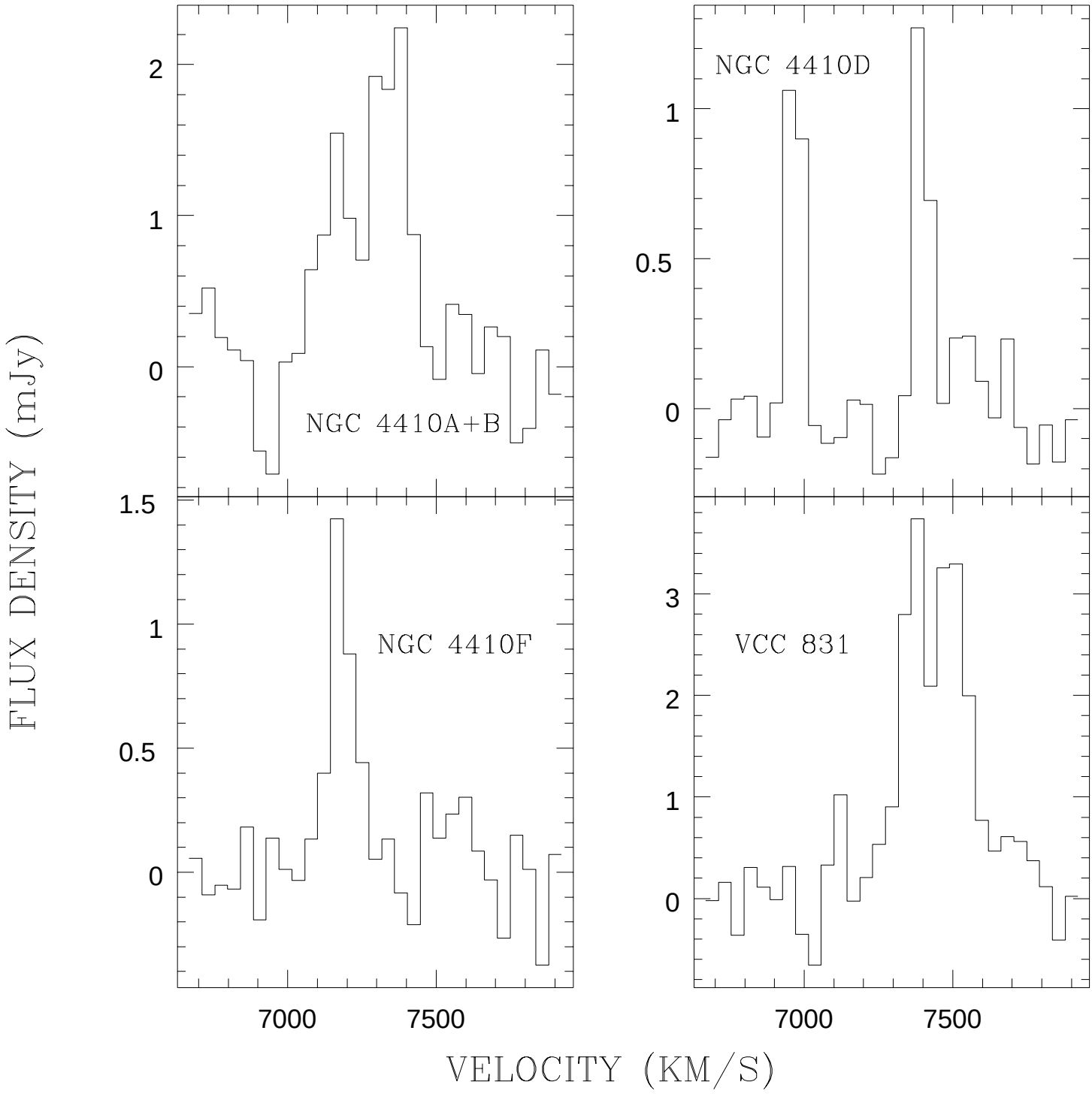
NGC 4410A+B
NGC 4410D
NGC 4410F
VCC 831
FLUX DENSITY (mJy)
VELOCITY (KM/S)
7000
7500

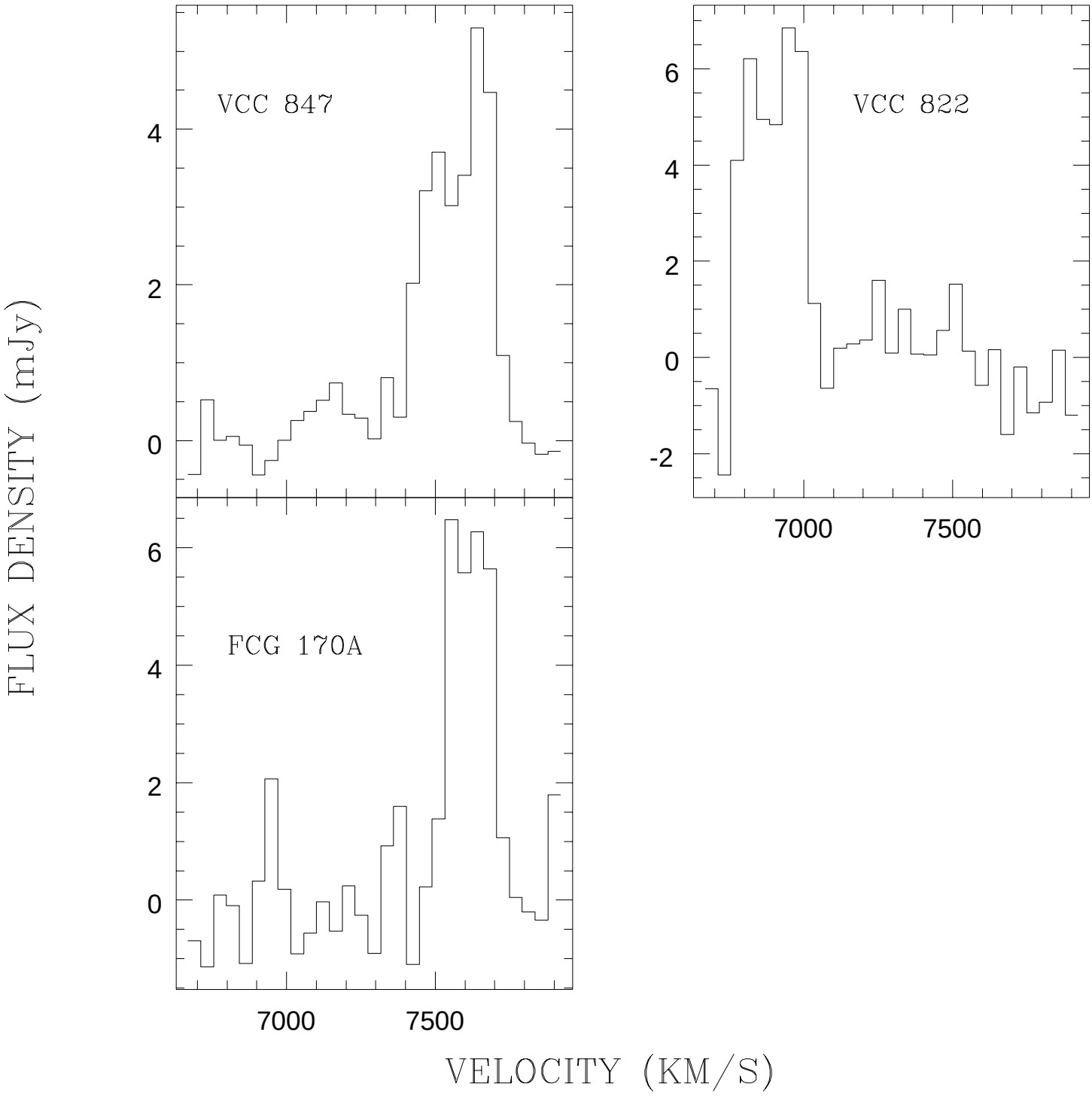
VCC 847
FCG 170A
VCC 822
FLUX DENSITY (mJy)
VELOCITY (KM/S)
7000
7500
0
2
4
6
-2

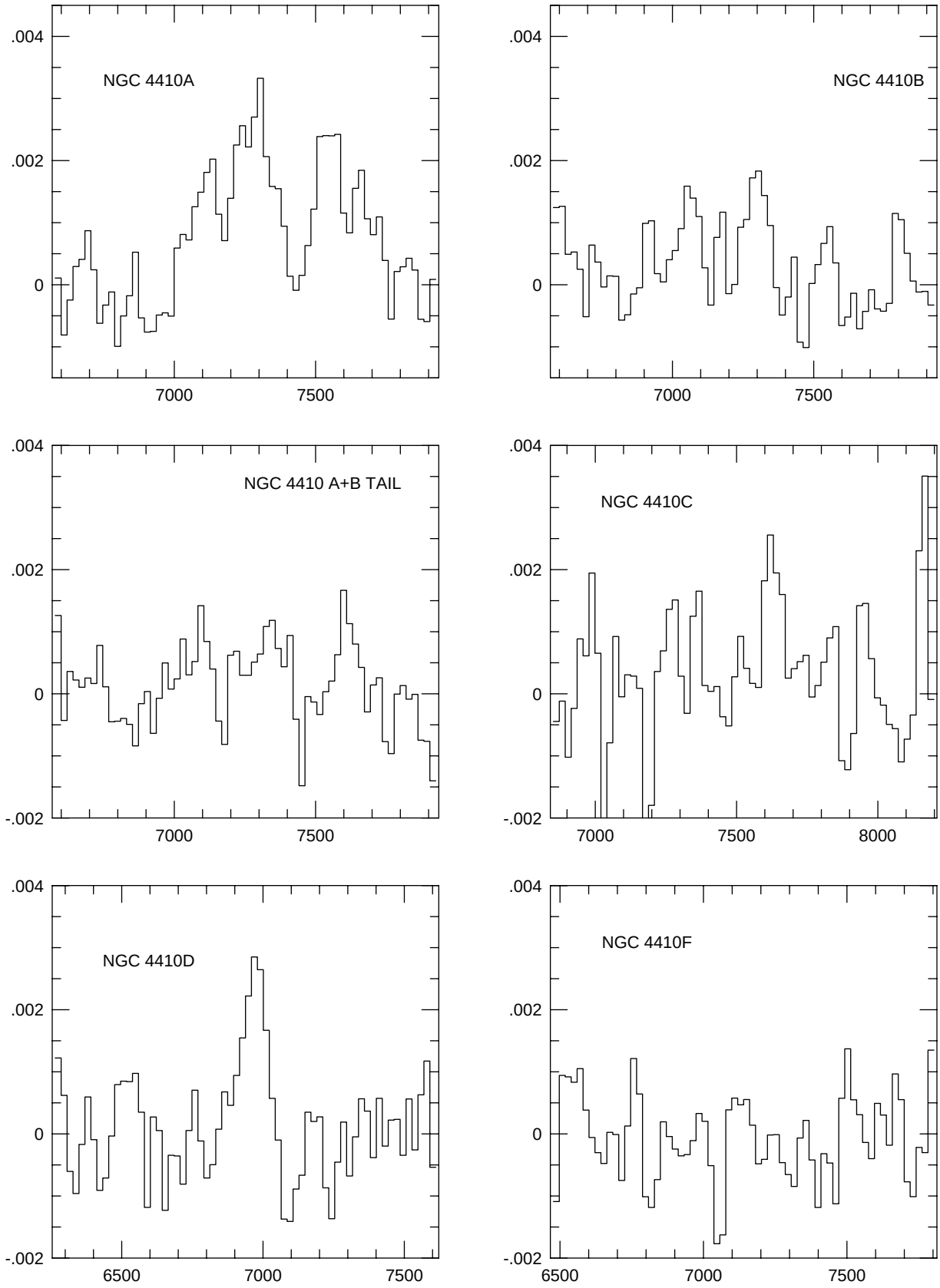


This figure "f8a.jpg" is available in "jpg" format from:
http://arXiv.org/ps/astro-ph/0005093

This figure "f8b.jpg" is available in "jpg" format from:

http://arXiv.org/ps/astro-ph/0005093

This figure "f8c.jpg" is available in "jpg" format from:

http://arXiv.org/ps/astro-ph/0005093

This figure "f8d.jpg" is available in "jpg" format from:

http://arXiv.org/ps/astro-ph/0005093